Molecular Dynamics Simulation of Homogeneous Crystal Nucleation in Polyethylene

Molecular dynamics simulation of homogeneous crystal nucleation in polyethylene

Peng Yi [1], C. Rebecca Locker[3], Gregory C. Rutledge [2]

[1]Department of Physics and [2]Department of Chemical Engineering

Massachusetts Institute of Technology, Cambridge, MA 02139, USA

[3]ExxonMobil Research and Engineering Company, Annandale, NJ 08801, USA

Abstract

Using a realistic united-atom force field, molecular dynamics simulations were performed to study homogeneous nucleation of the crystal phase at about 30% supercooling from the melts of *n*-pentacontahectane (C150) and a linear polyethylene (C1000), both of which are long enough to exhibit the chain folding that is characteristic of polymer crystallization. The nucleation rate was calculated and the critical nuclei were identified using a mean first-passage time analysis. The nucleation rate was found to be insensitive to the chain length in this range of molecular weight. The critical nucleus contains about 150 carbons on average and is significantly smaller than the radius of gyration of the chains, at this supercooling. A cylinder model was used to characterize the shape of the crystal nuclei and to calculate the interfacial free energies. A chain segment analysis was performed to characterize the topology of the crystal surface in terms of loops (including folds) and tails. The length distribution of loops is broad, supporting the "switchboard model" for the early stage crystals formed at deep supercooling. Using the survival probability method, the critical nucleus size was determined as a function of temperature. The interfacial free energies were found to be temperature-dependent. The free energy barrier and nucleation rate as functions of temperature were also calculated and compare favorably with experiments.

I. Introduction

The crystallization of polymers, like that of small molecules, can be described by a two-stage process of homogeneous nucleation and crystal growth. Significant understanding of the second stage, crystal growth, has been achieved as a result of several decades of investigation, using a variety of techniques including optical microscopy, light scattering, X-ray scattering, atomic force microscopy, calorimetry and molecular simulation; a number of texts and reviews are available.[1-9] However, the initial stage involving nucleation of polymer crystals has received much less attention, despite early efforts in this direction over 50 years ago.[10] Most of the previous studies of polyethylene that focused on homogeneous nucleation [10-14] relied on the droplet technique [15], where a volume of melt is dispersed into a large number of droplets, N_0. N_0 is chosen to be large so that only a small fraction of droplets contain impurities, and the droplets are small (on the order of micrometers) so that each droplet can accommodate only one nucleation event. Crystallization of droplets is often detected using optical microscopy, and the fraction of crystallized droplets N_C/N_0, is recorded as a function of time. The theoretical form of N_C/N_0 is known for steady-state nucleation under classical nucleation theory, and can be used to fit the experimental data to estimate kinetic and thermodynamic properties.[16] Many factors can affect the interpretation of the experimental results, including cooling rate, droplet sizes and their polydispersity, thermal history, effects of suspending media or substrates, and validity of the steady-state nucleation assumption.[17] As a result, given the relative paucity of experimental investigations, our understanding of the nucleation of polymer crystals on the microscopic level is sorely incomplete. For example, one very interesting phenomenon that is unique to polymer systems is chain folding during crystallization.[18, 19] Despite much experimental effort, it still remains unclear at what point during crystallization, and by what

mechanism, the characteristic folded configuration of lamellar polymer crystallites is realized during the liquid-to-solid transition. Compared to crystallization from solution, this problem is particularly complicated in crystallization from the melt, because the nucleation process and the subsequent thickening process, during which crystal nuclei grow in the chain axis direction, are difficult to separate. Nevertheless, chain folding and development of the lamellar crystalline morphology is essential to the structure and properties of the majority of commodity and high performance plastics.

Given the lack of spatial and temporal resolution of current experimental techniques, computer simulation offers a valuable alternative to improve our understanding regarding homogeneous nucleation. Furthermore, the study of homogeneous nucleation is particularly suited to molecular simulation because, firstly, the most interesting features are manifested on the nanometer length scale, and secondly, unlike experiments, simulation permits full control over the composition of the system to ensure impurity-free homogeneous nucleation conditions. However, homogeneous nucleation is also a rare event, which tends to be particularly challenging for compute-intensive molecular simulations, due to the potentially prohibitive waiting times between short bursts of interesting dynamics. To overcome this problem, it is common practice in molecular simulations of polymer crystallization to bias the simulation in a manner that reduces the waiting times or eliminates them altogether. Such approaches that have been used in the past include restriction to short chains[20-23], use of pre-oriented melts [24-27], artificially stiffening or linearizing the chain backbone [28, 29], coarse graining of the polymer chain beyond the level of united atoms [30-33], or surface-induced pre-ordering [34, 35]. In addition, high degrees of supercooling are normally employed to achieve nucleation rates high enough to observe nucleation in the much smaller volumes of simulation cells as compared to sample volumes used in experiments. Even

so, to our knowledge, there does not exist any simulation work that fully characterizes homogeneous nucleation in a polymer melt, complete with determination of the nucleation rate and identification of the transition state.

In this work, we study homogeneous crystal nucleation from the melt for the oligoethylene n-pentacontahectane (C150) and a short polyethylene (C1000). This is a continuation of our previous work for the normal alkanes *n*-octane (C8) and *n*-eicosane (C20).[22, 23] Our motivation for selection of C150 and C1000 for this study is two-fold. First, C150 is the shortest chain to display chain folded crystals (from solution).[18] Second, the entanglement length of polyethylene is about 60-80 carbons [36, 37]; C150 is about twice this length, thereby ensuring that the effects of entanglements on crystallization kinetics are captured. Both folding and entanglement are essential characteristics of polymer crystallization from the melt. This paper is organized as follows. We first present the theoretical background and analytical method, followed by simulation details. Then we will discuss our simulation results and compare with existing experimental studies.

II. Theory and method

Classical nucleation theory (CNT) has been widely used to describe homogeneous nucleation. The crystallites of chain molecules and polymers are necessarily anisotropic and exhibit at least two distinct types of surfaces: (i) chain-end or chain-folded surfaces, and (ii) lateral or side surfaces. For this reason, a cylinder model is often assumed to describe the shape of crystallites in polymer systems. Our recent studies of C8 and C20 confirm unambiguously that this is the simplest model that captures the shape of the free energy curve for homogeneous nucleation.[22, 23] The free energy of formation of a cylindrical crystal nucleus is given by

$$\Delta G = 2\pi r^2 \sigma_e + \pi r l \sigma_s - \pi r^2 l \Delta G_v , \quad (1)$$

where σ_e and σ_s are the interfacial free energies for the end and side surfaces of a cylindrical nucleus of radius r and length l, and ΔG_v is the Gibbs free energy difference per unit volume between the crystal and melt phases. For a small degree of supercooling $\Delta T/T_m$, ΔG_v can be approximated by $\Delta G_v \approx \rho_n \Delta H_f \Delta T/T_m$, where ρ_n is the molecule number density, ΔH_f is the heat of fusion per molecule at the thermodynamic equilibrium melting temperature T_m, and ΔT (equal to T_m-T) is the supercooling. For deeper supercooling, a more accurate approximation [38] is

$$\Delta G_v \approx \rho_n \Delta H_f T \Delta T / T_m^2 . \quad (2)$$

Minimizing ΔG with respect to r and l gives the critical radius r^* and critical length l^*, respectively.

$$\begin{cases} r^* = 2\sigma_s / \Delta G_v \\ l^* = 4\sigma_e / \Delta G_v \end{cases} . \quad (3)$$

Inserting the values of r^* and l^* into Eq. (1), we obtain the free energy barrier,

$$\Delta G^* = 8\pi \frac{\sigma_s^2 \sigma_e}{(\Delta G_v)^2} . \quad (4)$$

The critical nucleus size, measured in number of molecules, is

$$n^* = \rho_n \pi (r^*)^2 l^* = 16\pi\rho_n \frac{\sigma_s^2 \sigma_e}{(\Delta G_v)^3} = \frac{2\rho_n}{\Delta G_v} \Delta G^* . \quad (5)$$

According to transition state theory, the nucleation rate I (in number of events per unit volume per unit time) is given by

$$I = I_0 \exp(-\Delta G^* / k_B T) = A \exp(-E_d / k_B T) \exp(-\Delta G^* / k_B T), \quad (6)$$

where E_d is the activation energy for processes that transport chain segments to or from the nucleus, e.g. by diffusion, and A is a temperature independent prefactor.

For steady-state nucleation, in which the size distribution of nuclei is time-independent despite the fact that there is a constant net flux of molecules from smaller nuclei to larger ones, the induction time τ^* is the time elapsed before a critical nucleation event occurs. The nucleation rate can be calculated from $I=1/(\tau^* V)$, where V is the volume of the system.[39] The term "induction time" or "incubation time" is often used in crystallization studies to denote the time elapsed before the establishment of steady-state nucleation in a bulk;[4] it should not be confused with the induction time of classical nucleation theory, as employed here. A mean first-passage time (MFPT) analysis [40] can be applied to the largest nucleus, n_{max}, observed in MD simulations in order to estimate the induction time. This implies that n_{max} is taken to be the reaction coordinate for the nucleation process [16]. For a process with a sufficiently high barrier, $\Delta G^* >> k_B T$, the MFPT for n_{max} follows the equation

$$\tau(n_{max}) = 0.5\tau^*[1 + erf(Z\sqrt{\pi}(n_{max} - n^*))] + G^{-1}(n_{max} - n^*)H(n_{max} - n^*), \quad (7)$$

where n^* is the critical nucleus size, Z is the Zeldovich factor, G is the growth rate and H is the Heaviside function. The second term on the right hand side has been added to the original equation of Ref. [40] to account for finite crystal growth rates of post-critical nuclei, when $G >> n^*/\tau^*$ is not satisfied. The Heaviside function was used because growth is defined only after nucleation has occurred. An error function can be used for a smooth approximation of the Heaviside function, i.e.,

$$\tau(n_{\max}) = 0.5\tau^*[1 + erf(Z\sqrt{\pi}(n_{\max} - n^*))] + 0.5G^{-1}(n_{\max} - n^*)[1 + erf(C(n_{\max} - n^*))], \quad (8)$$

where $C \to \infty$ is chosen to be a large positive number in practice. This method has been applied to MD simulations of homogeneous crystal nucleation in two shorter *n*-alkane systems [22, 23] at about 20% supercooling.

MFPT analysis relies on an unbiased MD simulation of the reversible growth and shrinkage of the largest nucleus until such time as it crosses the free energy barrier and proceeds to grow irreversibly. At shallow supercooling, this is not practical because the free energy barrier increases with temperature according to Eq. (2) and (4), resulting in prohibitively long induction times for simulation studies close to T_m. Therefore, to calculate the critical nucleus size n^* at higher temperatures, we used a survival probability method[41]. According to CNT, the critical state, comprising the ensemble of configurations containing a critical nucleus, is a point of unstable equilibrium, with equal probability for a given configuration to evolve to either the fully crystallized or molten state. In the survival probability method, we prepare an ensemble of configurations in which the largest nucleus size is n_0 and then run MD simulations on each configuration at different temperatures. There exists one temperature T_c at which the configurations in the ensemble exhibit a 50% probability to crystallize (or melt); n_0 is then equated with the critical nucleus size at this T_c. This method has been previously applied with some success to the Ising model[41] and the Lennard-Jones system[42, 43].

III. Simulation details

As in our previous studies of C8 and C20, we used the united-atom force field originally proposed by Paul, Yoon and Smith (PYS) [44] and subsequently modified by Waheed *et al.*, [45, 46]. This force field combines the hydrogens and carbon of each CH_2 or CH_3 moiety into a

single united atom (UA) site, but otherwise retains all of the conformational degrees of freedom of a fully explicit atom model. It has been shown to reproduce a variety of melt phase structures and dynamical properties as well as the structure, melting point, and enthalpy of the rotator phase in short *n*-alkanes. It favors the hexagonal crystal phase of polyethylene over the more commonly observed orthorhombic crystal phase. Details of this force field may be found elsewhere [22]. MD simulations were performed using the open source LAMMPS package[47]. Isothermal-isobaric (NPT) ensembles were used with the pressure P=1atm. The equations of motion were integrated using the velocity Verlet method with an integration time step Δt=5fs. The details of the thermostat and barostat can be found in Yi and Rutledge [23].

The simulations used to characterize the amorphous melts and to study crystal nucleation were performed on systems containing either 60 C150 chains or 9 C1000 chains. The simulation cells were orthorhombic with the side lengths changing independently. Periodic boundary conditions were applied in all three directions to approximate bulk-like behavior. The initial configurations were generated at a density of 0.3g/cm^3 by randomly growing each chain with fixed bond lengths, fixed bond angles and torsion angles based on their energy distribution at 550K, similar to the method used by Waheed *et al.*[46]. These configurations were equilibrated at 550K for 100ns before being quenched instantaneously to a lower temperature for simulation of the amorphous phase or studies of nucleation.

The simulations used to characterize the crystal phase were performed on a system of 320 C150 chains. A triclinic simulation cell with all angles and side lengths varied independently was used, with periodic boundary condition in all three directions. The initial configurations were generated using a hexagonal lattice with a=0.48nm, and c=19.5nm. These configurations were

equilibrated at 200K for 20ns before being heated instantaneously to a higher temperature to simulate the crystal phase properties.

IV. Results and discussions

a. Properties of the amorphous and crystal phases

The glass transition temperature T_g was first estimated to identify the proper temperature range for crystallization simulation. An amorphous system was cooled at a finite cooling rate, and the specific volume as a function of temperature was monitored, as shown in Figure 1. The slope of this curve is the thermal expansion coefficient. A change of the thermal expansion coefficient indicates the apparent glass transition. The apparent glass transition is known to be cooling rate-dependent, so that the high cooling rates used in simulations generally lead to a higher estimate of T_g compared to experimental methods. To account for this, three different cooling rates were used, 100K/ns, 25K/ns and 10K/ns. A plot of apparent T_g versus cooling rate was then extrapolated to zero cooling rate, as shown in the inset of Figure 1, resulting in the estimate T_g^0=215.22±1.24K for C150. Following the same procedure, T_g^0 was found to be 223.04±0.22K for C1000, which is in good agreement with experimental values for polyethylene, 120K-220K, [48]. For comparison, a previous estimate of T_g using a smaller simulation of 4 C1000 chains, the same force field, a cooling rate of 125 K/ns and no extrapolation resulted in the estimate T_g(@125 K/ns)=280±32 K [49]. Other investigators also reported T_g between 200K and 250K using simulation methods.[50, 51] In the following studies, we carried out crystal nucleation simulations at 280K, which is well above T_g^0.

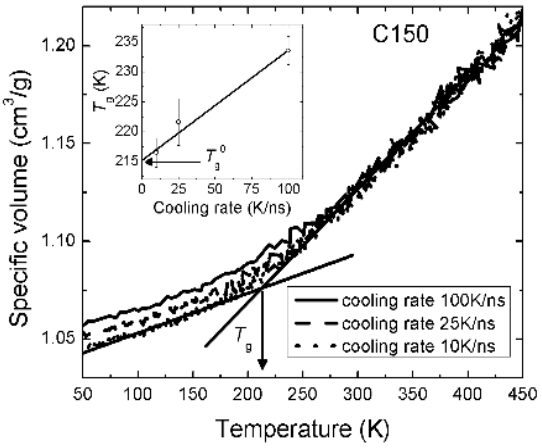

Figure 1. Specific volume as a function of temperature during cooling simulations at three different cooling rates, 100K/ns, 25K/ns and 10K/ns, respectively. (Inset) The glass transition temperature, T_g, as a function of cooling rate and the extrapolation of T_g to zero cooling rate.

MD simulations were performed on C150 melts at different temperatures to calculate the end-to-end vector orientation autocorrelation function and the mean square displacement (MSD) of the centers of mass of the chains, as described in [52]. These results are shown in Figure 2. From the slope of the logarithm of the end-to-end vector orientation autocorrelation function versus time, a characteristic relaxation time is obtained. This relaxation time is equated with the Rouse time τ_R, invoking the assumption that hydrodynamic interactions are screened in the melt. The supercooled melt shows significant slowdown as the Rouse time τ_R increases much faster than the $1/T$ predicted by the Rouse model. From the MSD we calculate the self-diffusion coefficient, MSD=$6Dt^{\nu}$, where ν is confirmed to be equal to unity at long time, according to Fick's law.[53] Our calculation shows that D=4.1×10^{-7} cm^2/s for C150 at 450K and 1atm, which agrees well with the empirical equation fitted from experimental data. [54] This value is slightly lower than that reported by Harmandaris *et al*. using a different UA force field [53], D≈7×10^{-7}cm^2/s for C156 at 450K and 1atm. The self-diffusion coefficients D obtained by simulations at several

different temperatures in the range 280-450K were fit to the equation $\ln D = \ln D_\infty - E_d/T$ where E_d is the activation energy for diffusion, as shown in the inset of Figure 2 (b). Our results show that E_d=21.46±3.30 kJ/mol, which agrees well with experiments.[54, 55] In the experiments [54-56], E_d attains an asymptotic limit for long chains, e.g., N>200 at T=423K [54]. This suggests that E_d is a measure of local relaxation and that the molecular weight dependence of D is mainly controlled by the parameter D_∞, i.e., $D_\infty(N)$.

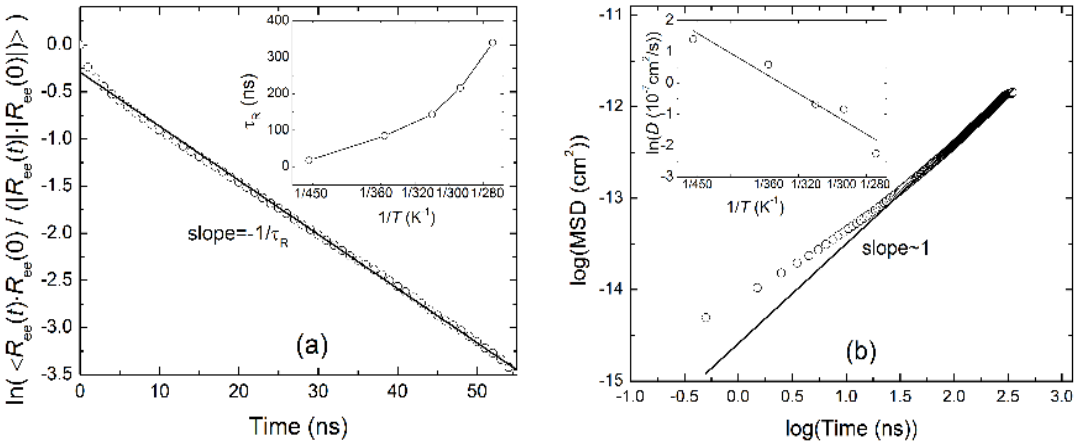

Figure 2. (a) End-to-end vector orientation autocorrelation function for C150 melt at 450K. Simulation data are shown with open circles and linear fitting is shown with a straight line. (Inset) Rouse time as a function of temperature for C150 melt. Line is provided as a guide to the eye. (b) Mean square displacements of center of mass of chains as a function of time for C150 melt at 450K. (Inset) Diffusion coefficient of center of mass of chains as a function of inverse temperature.

Potential energy per chain and average density were extracted from simulations of the melt phase and of the crystal phase for C150 at each temperature. These data, shown in Figure 3, were extrapolated to the experimentally determined equilibrium melting point T_m=396.4K [18] for the calculation of the heat of fusion $\Delta H_f = \Delta E + P\Delta V$. From ΔE=467.35±17.15 kJ/mol and ΔV=310.54±20.06 cm^3/mol, we obtain ΔH_f ≈467±17 kJ/mol of C150 molecules; this is equivalent to 53.1±1.9 cal/g, which can be compared with the experimental value of 68.4 cal/g

for polyethylene [57]. As was noted previously for *n*-eicosane[23], the simulated value is predictably lower than the experimental value, since the PYS force field predicts crystallization into a rotator phase rather than the experimentally observed orthorhombic crystal phase of polyethylene. It is worth noting, however, that the heat of fusion for the rotator phase of *n*-eicosane, which is observed experimentally, was accurately reproduced by simulations using the PYS force field.[23]

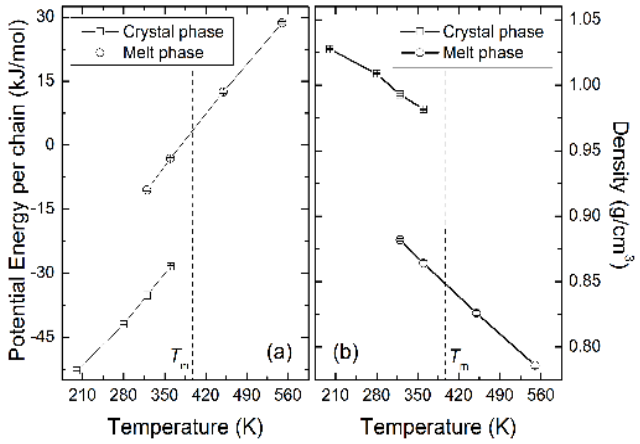

Figure 3. Temperature dependence of potential energy per chain (a), and average density (b), in the crystal phase and the melt phase in the simulated C150 systems. Dash lines indicate the melting temperature. Solid lines are provided as guides to the eye.

b. Homogeneous nucleation in C150 and C1000 melts

Figure 4 (a) shows plots of potential energy and n_{max} versus time from a representative MD trajectory of a C150 melt undergoing homogeneous crystal nucleation at 280K. Three distinct time periods are observed: (1) re-equilibration of potential energy in the first ~25 ns after quenching; (2) an induction period between 25 ns and 200 ns, during which time small fluctuations in both energy and n_{max} are observed; and (3) nucleation and growth of a stable crystallite after ~200 ns. Using independent starting configurations, 16 trajectories for C150, and

10 trajectories for C1000, were collected, from which the mean first-passage time of n_{max} was obtained for both C150 and C1000, as shown in Figure 4(b). Eq.(8) was fitted to each of these curves, as shown in Figure 4(b), for the estimation of induction time τ^*, the critical nucleus size n^*, the Zeldovich factor Z and the growth rate G. The parameter C in Eq.(8) was fixed to a large number during the fitting process. When C is greater than 100, the values of τ^*, n^*, Z and G are invariant with C; they are reported in Table 1.

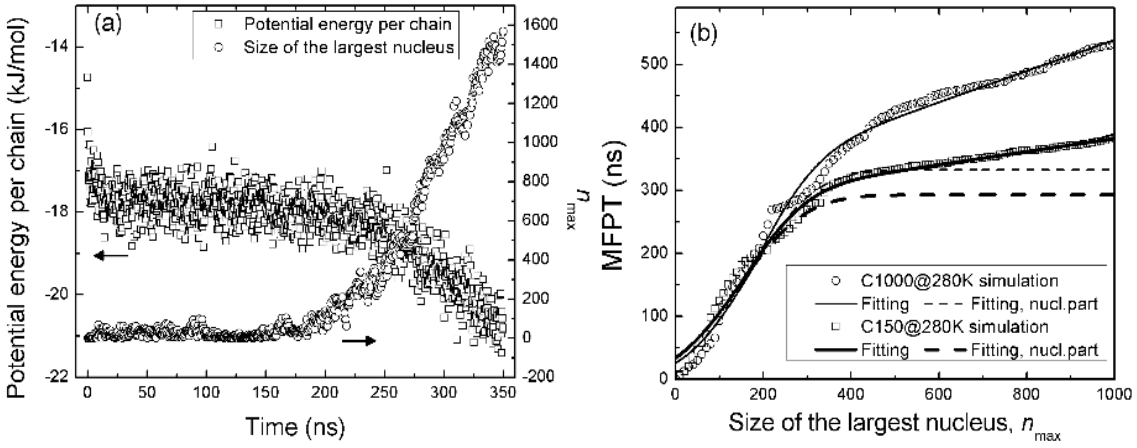

Figure 4. (a) Potential energy and the largest nucleus size, n_{max}, as functions of time during a typical MD trajectory of homogeneous crystal nucleation in C150 melt. The system was quenched from 550K to 280K at time 0; (b) MFPT for C150 and C1000 at 280K.

Table 1. The fitting results of MFPT to Eq.(7) for C150 and C1000 at 280K

system	Z ($\times 10^{-3}$)	n^* (UA)	τ^* (ns)	I (10^{25} $s^{-1}cm^{-3}$)	G (UA/ns)
C150	5.9 ± 0.1	143 ± 1	293 ± 2	1.47 ± 0.01	9.6 ± 0.2
C1000	6.0 ± 0.1	167 ± 1	333 ± 2	1.31 ± 0.01	4.0 ± 0.1

Remarkably, we find that the nucleation rates are almost identical for C150 and C1000 at 30% supercooling, and are only about a factor of four slower than that obtained previously for C20 at 20% supercooling. This confirms that nucleation is a local event. At such deep supercooling, nucleation is not affected strongly by the molecular weight, but only by the local environment. The snapshot in Figure 5 shows that even a post-critical nucleus of size 800 UAs engages only relatively short segments of numerous C150 chains. In contrast to the nucleation rate, the growth rate differs considerably between C150 and C1000. Our observation of the molecular weight independence of nucleation rate is consistent with droplet experiments. Cormia *et al.* [10] found that at deep supercooling the kinetic prefactor I_0 was not significantly different between PE and *n*-alkane, therefore the chain segments involved in the diffusion processes must be similar in PE and in *n*-alkane. Massa *et al.* [58] also found for poly(ethylene oxide) that the homogeneous nucleation rate is independent of molecular weight. Some experimental studies of polymer solution crystallization [59, 60] have been used to argue that nucleation rate is inversely proportional to molecular weight. However, it should be noted that these studies likely involved heterogeneous nucleation, and that the thermodynamic free energy barrier is nevertheless M_w-independent, since the nuclei are much smaller than the chain size. Thus the nucleation prefactor must contain a M_w-dependent factor, which was attributed to the diffusivity D, in order to explain the experimental observations. These observations and our simulations can be rationalized if one realizes that the experimentally observable "nuclei" are much bigger than the critical nucleus size predicted by simulation. We posit that, due to limited spatial and temporal resolution of the methods, the experimentally observed nuclei are in fact post-critical crystallites, the development of which is sensitive to the molecular weight dependence of the growth process. While it is common to include the diffusivity D, or sometimes viscosity η, in the nucleation prefactor I_0 for

simple liquids, our simulations indicate that this cannot be the case for polyethylene, at least at 30% supercooling. Instead, the nucleation prefactor must depend on a segmental motion that is localized and not molecular weight dependent.

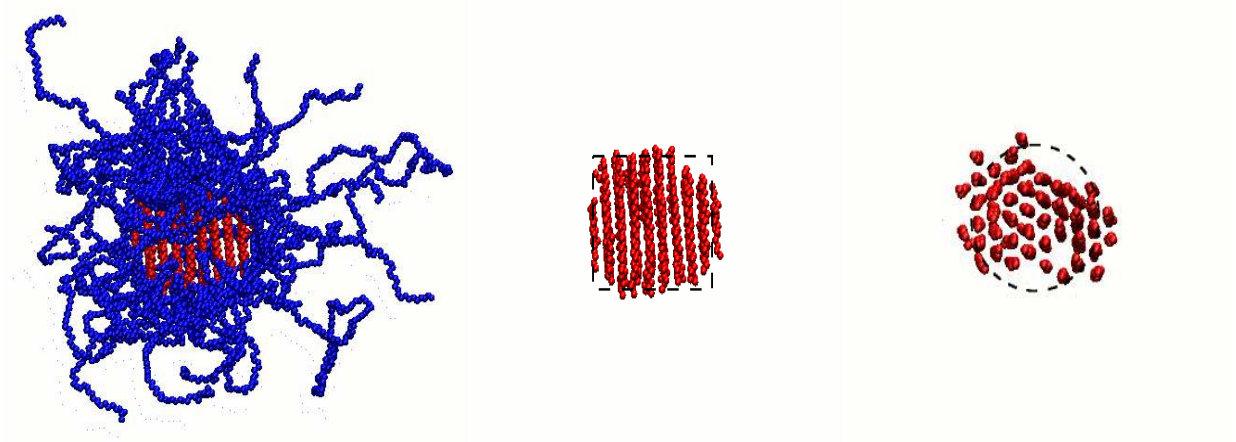

(a) (b) (c)

Figure 5. Snapshot of a crystal nucleus of size 800 in a supercooled C150 melt. (a) Only chains that participate the nucleus are shown. The UAs in the crystal nucleus are shown in red while the UAs that are in the melt phase are shown in blue. (b) Only UAs that are in the nucleus are shown (side view). (c) Only UAs that are in the nucleus are shown (top view). A cylinder shape illustrated by black dash lines is provided as a guide for the eye.

The shape of the crystal nuclei is characterized using the cylinder model. The stem length, or thickness, of crystal nuclei l was calculated as a function of nucleus size n and is shown in Figure 6 (a). Fitting this data to a power law produces a scaling coefficient of 0.31, which is close to 1/3 and suggests that small nuclei grow in three dimensions. Finding l^* for n^* at 280K, we calculated the interfacial free energies to be σ_s=21.4 mJ/m^2 and σ_e=12.4 mJ/m^2 at 280K. These values are higher than those previously calculated for C8 and C20[22, 23], a trend that is consistent with experiments.[61] The amorphous chain segments attached to the crystal nuclei

tend to repel each other because of the lower density in the melt. This repulsion creates excess stress on the interface, which increases as the length of the amorphous segments increases.

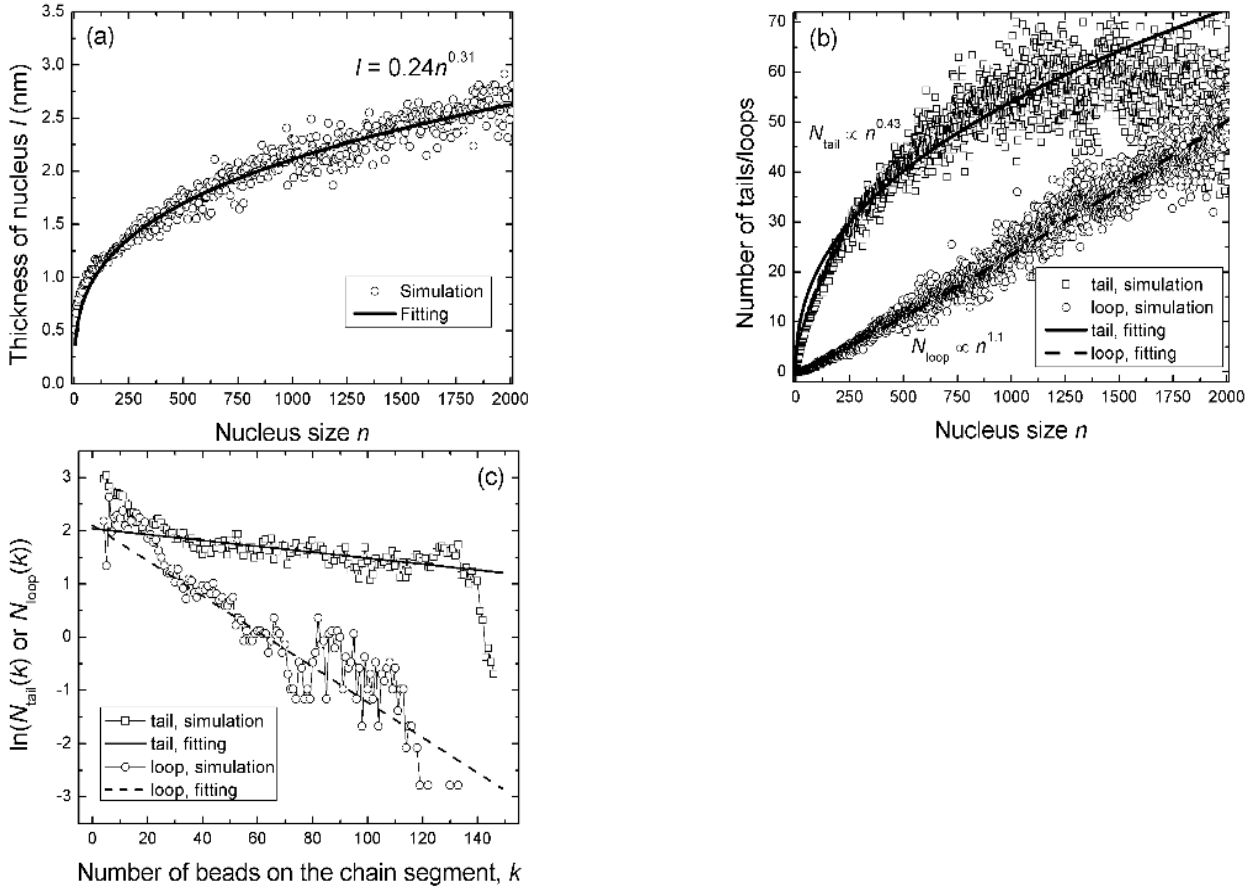

Figure 6. (a) Thickness of cylindrical crystal nucleus as a function of nucleus size; (b) number of tails and loops as functions of nucleus size; (c) Number of tails and loops as functions of their respective contour lengths, for nuclei of size about 800 UAs.

We also characterized topology of the crystal surface in terms of these amorphous chain segments, in particular loops and tails that belong to chains with segments incorporated into the nuclei. A loop is defined as an amorphous chain segment that connects two crystal stems in the same nucleus, and a tail is defined as an amorphous chain segment with one end attached to one crystal nucleus and the other end free in the melt. The term "fold" is reserved here for a loop

with fewer than 10 carbons. As shown in Figure 6 (b), the number of tails and loops, N_{tail} and N_{loop}, scale with the size of the nucleus as $N_{tail} \sim n^{0.43}$ and $N_{loop} \sim n^{1.1}$, respectively. Since the number of UAs in the nucleus is proportional to the nucleus volume, the cross-sectional area of the cylindrical nuclei, S, is proportional to n/l.Then according to Figure 6(a), S is proportional to $n^{0.69}$, and N_{tail} and N_{loop} are proportional to $S^{0.62}$ and $S^{1.6}$, respectively. For small nuclei, tails are more common than loops; as nuclei increase in size, the likelihood that two or more stems belong to the same chain increases, thereby accounting for the stronger dependence of N_{loop} on cylinder area S. It is clear that N_{tail} is much greater than 2 even when nucleus size $n < 100$ UAs, suggesting that there are multiple chains participating in the crystal nucleus during the critical nucleation event, rather than a single chain as suggested by the "intramolecular nucleation" mechanism. [62, 63]

The contour length distributions of tails and loops, $N_{tail}(k)$ and $N_{loop}(k)$, are also calculated for nuclei of size 800±25 UA. It is clear from Figure 6 (c) that both types of segments have broad distributions of length. This finding supports the "switchboard" re-entry model proposed by Flory and Yoon [64], at least for early stage crystallites at deep supercooling. The contour length distribution of both tails and loops shows an exponential decay as a function of contour length, suggesting a constant incremental potential for each UA on polymer chains. From the slopes of the curves in Fig 6(c) for $k>30$, values of –0.013 kJ/mol and –0.077 kJ/mol may be estimated for the incremental chemical potentials of tails and loops, respectively. These values can be compared to $\mu_{UA}^{sim} \sim -0.033$ kJ/mol obtained from simulations of melts of linear alkanes at P=1.02 atm [65], $\mu_{UA}^{expt} \sim -0.039$ kJ/mol from fitting of experimental data using the Peng-Robinson equation of state[66] and $\mu_{UA}^{sim} \sim -0.03$ kJ/mol obtained from Monte Carlo simulation of interlamellar isotactic polypropylene.[67] The difference between the values for incremental

chemical potential of loops and tails estimated here, and the values determined from melts, presumably traces back to the relatively random nature by which segments of chains are incorporated kinetically into the nucleus.

c. Temperature dependence of nucleation rate for C150

The survival probability method was used to determine the temperature dependence of the critical nucleus size. MD simulations were performed using ensembles of C150 systems with initial values of n_{max}=150, 200, 400, 600, and 800 UAs, respectively. Each ensemble contained 8 different initial configurations. The initial configurations were extracted from the previous MD simulations used to observe nucleation at 30% supercooling. Figure 7 (a) shows one set of simulations with an initial n_{max}=400 at four different temperatures, 280K, 290K, 300K and 310K. The system melted at 300K and 310K, and crystallized at 280K and 290K. From this one concludes that the critical nucleus size n^* is bigger than 400 at temperatures greater than or equal to 300 K, and smaller than 400 at temperatures less than or equal to 290 K. If this trend holds, at some temperature T_c between 290K and 300K we should have n^* equal to 400. For each ensemble, the probability of melting was fitted to an error function to estimate T_c, as illustrated in Figure 7 (b). In this way, we determined the critical nucleus size n^* as a function of temperature; this is plotted in Figure 7 (c).

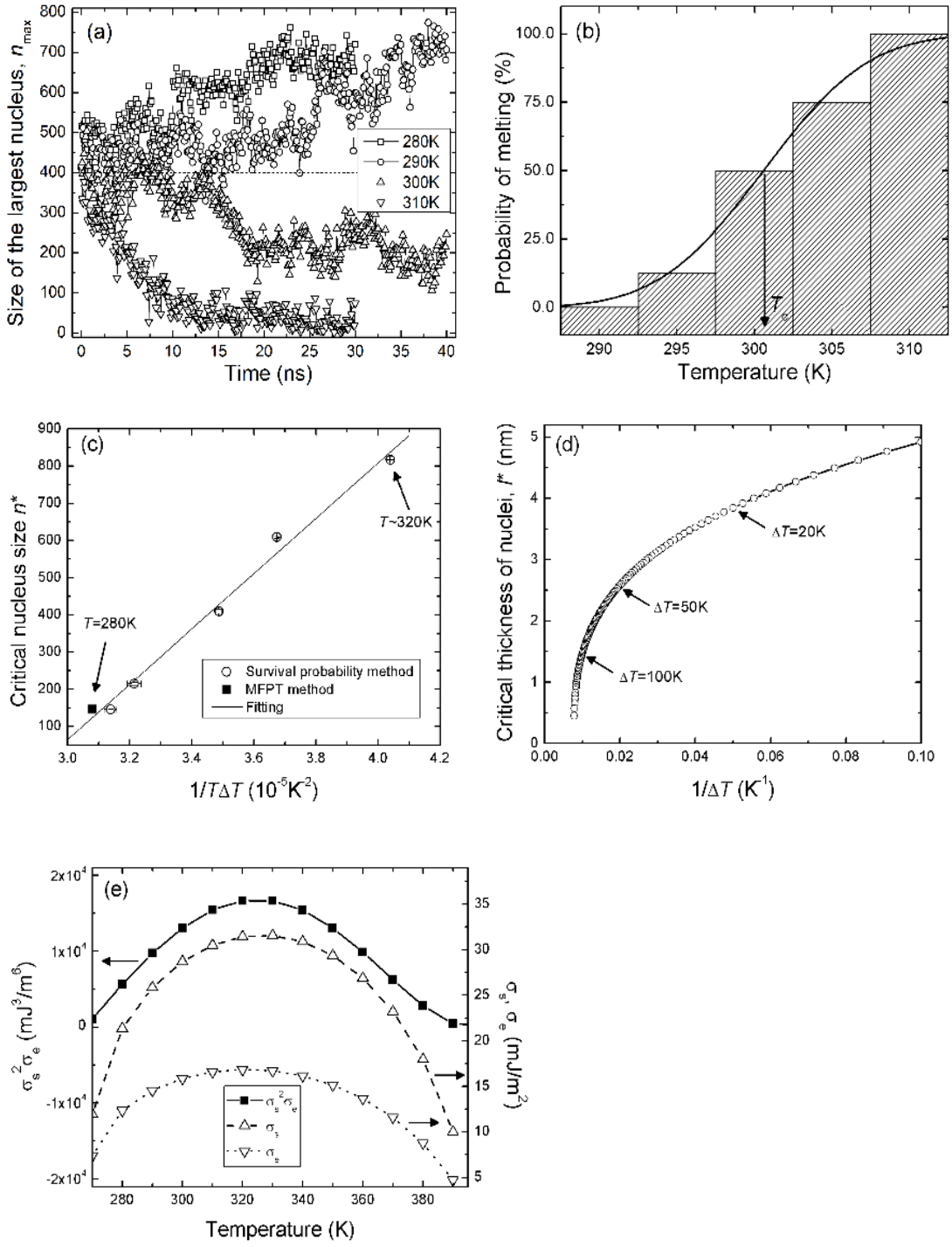

Figure 7. (a) MD simulations of C150 melts at different temperatures using the same initial configuration with n_{max}=400 UA; (b) Probability of melting at different temperatures with an initial n_{max}=400; (c) Critical nucleus size n^* as a function of $(T\Delta T)^{-1}$ for C150 melts; (d) Calculated critical thickness of nucleus as a function of supercooling; see text for details; (e) Calculated interfacial free energies as a function of temperature; see text for details.

As shown in Figure 7 (c), n^* as a function of temperature is well described by an equation of the form $n^*=a+b/T\Delta T$; the fitting parameters for C150 are determined to be a=–2164±129 UAs and b=(7.43±0.37) $\times 10^7$ UAs·K^2. Assuming that the functional dependence expressed by Figure 6 (a) is invariant with temperature and using Figure 7 (c), the thickness, l^*, of the critical nucleus can be estimated for C150 at any temperature, as shown in Figure 7(d). This l^* is approximately linear with $1/\Delta T$ at small supercooling. However, it should not be mistaken for the lamellar thickness often discussed in the context of crystal growth, which corresponds to the fastest lateral growth rate and has also been shown to be proportional to $1/\Delta T$, or to $1/T\Delta T$ if better approximation is desired at deep supercooling (Eq.(2)). Here the critical thickness l^* might be related to the initial lamellar thickness discussed by Barham *et al*.[68]; it indicates at what temperature crystallites with a certain thickness can form. For example, equating l^* from Figure 7(d) with half the contour length of the fully extended C150 chain, one can obtain an estimate of ΔT=2K for the supercooling at which a once-folded critical nucleus of C150 would be observed. Based on this estimate, any supercooling deeper than 2K should result in once- or multiply-folded crystallites, yet folded C150 crystallites are not observed in melt crystallization experiments. That is probably because the isothermal thickening rate is fast on the time scale of observation. As a rough estimate, assuming that the crystal nucleus size n increases linearly with time at the growth rate G estimated in the foregoing MFPT analysis, then the time needed for a crystal nucleus of C150 chains to reach the extended chain thickness is on the order of 10^{-4} sec, while that for C1000 chains is on the order of 10^{-1} sec. Thus, as the chain length increases, folded chain crystallites become kinetically stabilized and are thus more likely to be observed.

According to Figure 7 (c), n^* is found empirically to vary linearly with $(T\Delta T)^{-1}$. This contrasts with the linear dependence on $(T\Delta T)^{-3}$ observed for crystallization of the simple Lennard-Jones

system, where the interfacial free energies are temperature independent[43]. Figure 7 (e) shows the product of interfacial free energies $\sigma_s^2\sigma_e$ as a function of temperature calculated based on the data of Figure 7 (c), Eq. (2) and Eq. (5). Furthermore, Figure 7 (d) and Eq. (3) were used to calculate σ_e individually; σ_s and σ_e can then be separated, and are also shown in Figure 7 (e). This analysis indicates that the temperature dependence is much more significant in C150 than in our previous simulation with short *n*-alkanes, and non-monotonic – the interfacial free energies take a maximum value at around 320K. One possible explanation is that there are significant and nontrivial energetic and entropic contributions arising from the onset of chain folding and looping. As shown previously, the numbers of tails and loops scale with the area of the end surface as $S^{0.62}$ and $S^{1.6}$, respectively. Therefore for the larger critical nuclei that are associated with higher crystallization temperature, loops are more common. Loops, and folds in particular, give rise to some crowding in the interface and a rise in the internal energy contributions to interfacial free energy.[69] However, at still higher temperatures, the topological entropy due to the introduction of loops and folds becomes important, eventually offsetting the internal energy contributions so that the effective interfacial free energy decreases with increasing nucleus size at high temperature. This behavior distinguishes the critical nuclei of C150 and polyethylene from the bundle-like nucleus previously reported for C20.[23]

Figure 8 (a) shows the free energy barrier ΔG^* calculated using classical nucleation theory (Eq.(2) and (5)) from the linear relation in Figure 7(c), based on the values of n^* obtained by survival probability analsysis. To calculate the nucleation rate by Eq.(6) over the range of temperatures, we only require the values of E_d and A. E_d has already been calculated from data in Figure 2 (a) and shown to be chain length independent. We note from Figure 8 (a) that the free energy barrier ΔG^* is about 40 kJ/mol at 280K, but drops to 8 kJ/mol at 270K, while the activation

energy E_d=21.46 kJ/mol. Therefore we expect the kinetic contribution to become rate-limiting for temperatures less than about 270-280K for C150. Given that E_d is M_w-independent for sufficiently long chains, this temperature might serve as a general lower limit of temperature for the application of CNT. The constant A can be determined by calibrating the nucleation rate to the simulation result at 280K, which gives A=4.3×10^{36} cm^{-3}sec^{-1}. The kinetic prefactor I_0=Aexp(−E_d/$k_B T$) is then calculated to be at 4.2×10^{32} cm^{-3}sec^{-1} at 280K. Combining the result of ΔG^*, E_d and A, the nucleation rate as a function of temperature is calculated as shown in Figure 8(b).

In contrast with the case for simple liquids, the growing/shrinking of crystallites during the nucleation process does not require the diffusion of the entire chains, particularly at deep supercooling. The nucleation prefactor I_0 therefore depends only on a segmental diffusivity D_{seg}. However, the temperature dependence, i.e., exp(−E_d/$k_B T$), remains in effect as the temperature changes the rate of diffusion. Other temperature insensitive factors are relegated to the factor A. We postulate that this characteristic segment length is limited by the mesh size created between entanglements, and the relevant dynamics scale with the Rouse dynamics of chain segments of entanglement length.[70, 71] Further investigation is required to identify the characteristic segment length as a function of temperature during polymer nucleation, and thereby provide a physical interpretation for A.

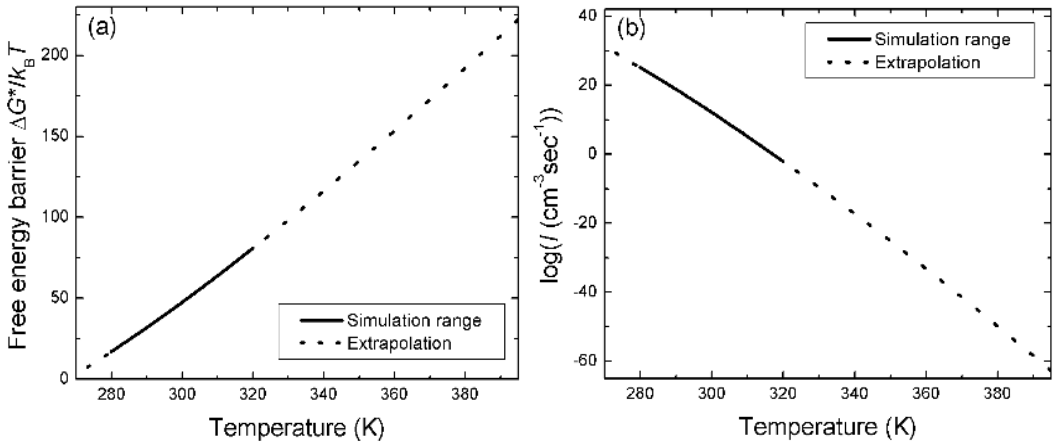

Figure 8. (a) Free energy barrier ΔG^* as a function of temperature; (b) nucleation rate I as a function of temperature.

d. Comparison to experiments

The experimental results for homogeneous crystal nucleation from the melt are rare for long *n*-alkanes or polyethylene; a number of these are summarized in **Error! Reference source not found.**. The experimental measurements of $\sigma_s^2\sigma_e$, the product of interfacial free energies, vary by a factor of 2 to 3. Our simulation results are of the same order of magnitude, with $\sigma_s^2\sigma_e$=5636 mJ/m^2 at 280 K, 15435 mJ/m^2 at 340 K and 9880 mJ/m^2 at 360K.

Table 2. The experimental estimates of nucleation kinetic prefector, I_0, and the product of interfacial free energies, $\sigma_s^2\sigma_e$, as compared with our simulation result.

Reference	System	T_c (K)	ΔT (K)	I_0 ($cm^{-3}sec^{-1}$)	$\sigma_s^2\sigma_e$ (mJ^3/m^6)
Cormia *et al*. [10]	PE	360	55	$10^{30.1}$	15500
Gornick *et al.* [11]	PE	362	53	10^{47}	14960
Koutsky *et al.* [12]	PE	360	55	2×10^{25}	6800
Ross and Frolen [13]	PE	358	57	$10^{49.4}$	19000
Kraack et al.[14]	~C140	349	47.6	10^{38}	6349
this work	C150	280 K	116.4	4.2×10^{32}	5636*

*: See text for different values at other temperatures.

It is not generally possible to obtain values of σ_s and σ_e individually from nucleation experiments. A second experiment is required. One common approach is to measure the initial lamellae thickness as a function of supercooling to derive the value of σ_e based on a kinetic theory.[2, 68] A second approach is to measure the melting temperature of lamellae as a function of lamellar thickness to derive the value of σ_e, based on the Gibbs-Thomson equation.[2] Both methods have yielded values of σ_e~90 mJ/m^2, which is significantly larger than our result of σ_e=12.4 mJ/m^2 at T=280 K. We believe the difference is attributable to the mature nature of the lamellae used in these latter experiments, in contrast to the nm-sized nuclei relevant during nucleation. This difference was also observed by Okada *et al*.[72], who measured the nucleus size distribution by SAXS technique and reported σ_e =18.5 mJ/m^2, in closer accord with our value of 12.4 mJ/m^2. Okada *et al.* hypothesized that σ_e increases to ~90 mJ/m^2 as the crystal lamellae grow, a process during which the surface topology changes. The determination of σ_s from

experiments is even less straight forward and requires certain approximations. The value of σ_s calculated from the characteristic ratio C_∞ is in the range of 10-20 mJ/m^2.[73, 74] Our value of σ_s = 21.4 mJ/m^2 at T=280K is slightly higher than this range.

Our simulation results of I_0 also fall within the range of experimental data, although it should be noted that the range of experimental measurements is quite large. The experiments are known to be extremely sensitive to any residual ordering that survived the melting process. It is more difficult to get a reliable estimate of I_0 than the interfacial free energies from experiments. Fast scanning DSC methods currently under development may offer an alternative means for measuring nucleation rates, but results for polyethylene are not yet available.[75] Crystallization of block copolymers could also provide an alternative to the classical droplet technique for studies of homogeneous nucleation.[76]

V. Conclusions

We have demonstrated that it is feasible to observe homogeneous nucleation of the crystal phase from the polyethylene melt at deep supercooling using molecular dynamics. This is attributed to the finding that the crystal nuclei are small relative to the radii of gyration of the chains, suggesting that polymer crystal nucleation is a local event. The nucleation behavior (dynamics and structure) itself is insensitive to chain length under these conditions. The growth rate, on the other hand, clearly decreases as the chain length increases. Based on this chain length independence, we postulated that the important unit during polymer crystal nucleation is a sub-chain segment, the length of which is selected by temperature and possibly entanglements; when the thickness of the nucleus exceeds the mesh size of the entanglement network, extrapolations such as the one shown in Figure 8 are likely to become inaccurate.

We characterized the shape of crystal nuclei using a cylinder model. For the deep supercooling employed here, the initial thickness of the critical nucleus is much shorter than the chain length, and the crystal stems are contributed by multiple chains, in contrast to the "intramolecular nucleation" mechanism. Amorphous chain segments form tails and loops that are attached to crystal nuclei. Both the tails and the loops have broad length distributions and suggest that the UAs on the chains have constant incremental potential.

The survival probability method was used to study critical nuclei over a broad range of temperatures. The thickness of the critical nucleus decreases with increasing supercooling, which might account for the onset of chain folding and looping with decreasing crystallization temperature or increasing molecular weight. The interfacial free energies were calculated using a cylinder model and found to be temperature dependent, with a maximum at about 320K. Although we observed that the crystal growth process is 3-dimensional immediately beyond the critical nucleation event, the ultimate shape of the crystal lamella is still expected to result from a competition between the thickening rate and the lateral growth rate, which diverge from each other as the crystallite grows.

Within the framework of classical nucleation theory, we have calculated the free energy barrier and its dependence on temperature. The diffusive and energetic contributions to the nucleation rate could thus be separately evaluated. By so doing, this work provides the first quantitative model of homogeneous nucleation of a polymer melt from first principles; it exhibits satisfactory agreement with existing experimental results. The simulations and theoretical analysis performed in this work constitute a set of methodologies that serve not only to reveal the molecular mechanisms underlying homogeneous crystal nucleation but also generate meaningful rate equations that can be used for engineering design purposes. It is our hope that the results

presented here prove to be both enlightening and of practical utility to the polymer crystallization community.

Acknowledgments

This work used the Extreme Science and Engineering Discovery Environment (XSEDE), which is supported by National Science Foundation grant number OCI-1053575. We appreciate many helpful discussions with Dr. Andy Tsou. Financial support from Exxon-Mobil is gratefully acknowledged.

References:

1. Schultz, J.M., *Polymer crystallization : the development of crystalline order in thermoplastic polymers*. 2001, Washington, D.C. : American Chemical Society.
2. Hoffman, J.D. and R.L. Miller, *Kinetic of crystallization from the melt and chain folding in polyethylene fractions revisited: theory and experiment.* Polymer, 1997. **38**(13): p. 3151-3212.
3. Strobl, G., *Crystallization and melting of bulk polymers: New observations, conclusions and a thermodynamic scheme.* Progress in Polymer Science, 2006. **31**(4): p. 398-442.
4. Long, Y., R.A. Shanks, and Z.H. Stachurski, *Kinetics of polymer crystallisation.* Progress in Polymer Science, 1995. **20**(4): p. 651-701.
5. Tashiro, K. and S. Sasaki, *Structural changes in the ordering process of polymers as studied by an organized combination of the various measurement techniques.* Progress in Polymer Science, 2003. **28**(3): p. 451-519.
6. Schick, C., *Differential scanning calorimetry (DSC) of semicrystalline polymers.* Analytical and Bioanalytical Chemistry, 2009. **395**(6): p. 1589-1611.
7. Hobbs, J.K., O.E. Farrance, and L. Kailas, *How atomic force microscopy has contributed to our understanding of polymer crystallization.* Polymer, 2009. **50**(18): p. 4281-4292.
8. Mandelkern, L., *Crystallization kinetics of homopolymers: overall crystallization: a review.* Biophysical Chemistry, 2004. **112**(2â€“3): p. 109-116.
9. Waheed, N., M. Ko, and G. Rutledge, *Atomistic Simulation of Polymer Melt Crystallization by Molecular Dynamics*, in *Progress in Understanding of Polymer Crystallization*, G. Reiter and G. Strobl, Editors. 2007, Springer Berlin / Heidelberg. p. 457-480.
10. Cormia, R.L., F.P. Price, and D. Turnbull, *Kinetics of Crystal Nucleation in Polyethylene.* The Journal of Chemical Physics, 1962. **37**(6): p. 1333-1340.

11. Gornick, F., G.S. Ross, and L.J. Frolen, *Crystal nucleation in polyethylene: The droplet experiment.* Journal of Polymer Science Part C: Polymer Symposia, 1967. **18**(1): p. 79-91.

12. Koutsky, J.A., A.G. Walton, and B. Eric, *Nucleation of Polymer Droplets.* Journal of Applied Physics, 1967. **38**(4): p. 1832-1839.

13. Ross, G.S.F., Lois J. , *Homogeneous nucleation in polyethylene: Molecular weight dependence.* Journal of Research of the National Bureau of Standards. Section A: Physics and Chemistry, 1975. **79A**(6): p. 701-711.

14. Kraack, H., E.B. Sirota, and M. Deutsch, *Homogeneous crystal nucleation in short polyethylenes.* Polymer, 2001. **42**(19): p. 8225-8233.

15. Vonnegut, B., *Variation with temperature of the nucleation rate of supercooled liquid tin and water drops.* Journal of Colloid Science, 1948. **3**(6): p. 563-569.

16. Yi, P. and G.C. Rutledge, *Molecular Origins of Homogeneous Crystal Nucleation.* Annual Review of Chemical and Biomolecular Engineering, 2012. **3**(1): p. 157-182.

17. Herhold, A.B., et al., *Impurity mediated nucleation in hexadecane-in-water emulsions.* Physical Review E, 1999. **59**(6): p. 6946-6955.

18. Ungar, G., et al., *The Crystallization of Ultralong Normal Paraffins: The Onset of Chain Folding.* Science, 1985. **229**(4711): p. 386-389.

19. Keller, A., *A note on single crystals in polymers: Evidence for a folded chain configuration.* Philosophical Magazine, 1957. **2**(21): p. 1171-1175.

20. Esselink, K., P.A.J. Hilbers, and B.W.H. van Beest, *Molecular dynamics study of nucleation and melting of n-alkanes.* The Journal of Chemical Physics, 1994. **101**(10): p. 9033-9041.

21. Takeuchi, H., *Structure formation during the crystallization induction period of a short chain-molecule system: A molecular dynamics study.* The Journal of Chemical Physics, 1998. **109**(13): p. 5614-5621.

22. Yi, P. and G.C. Rutledge, *Molecular simulation of crystal nucleation in n-octane melts.* The Journal of Chemical Physics, 2009. **131**(13): p. 134902.

23. Yi, P. and G.C. Rutledge, *Molecular simulation of bundle-like crystal nucleation from n-eicosane melts.* The Journal of Chemical Physics, 2011. **135**(2): p. 024903-11.

24. Koyama, A., et al., *Molecular dynamics simulation of polymer crystallization from an oriented amorphous state.* Physical Review E (Statistical, Nonlinear, and Soft Matter Physics), 2002. **65**(5): p. 050801-4.

25. Lavine, M.S., N. Waheed, and G.C. Rutledge, *Molecular dynamics simulation of orientation and crystallization of polyethylene during uniaxial extension.* Polymer, 2003. **44**(5): p. 1771-1779.

26. Ko, M.J., et al., *Characterization of polyethylene crystallization from an oriented melt by molecular dynamics simulation.* The Journal of Chemical Physics, 2004. **121**(6): p. 2823-2832.

27. Jabbarzadeh, A. and R.I. Tanner, *Crystallization of alkanes under quiescent and shearing conditions.* Journal of Non-Newtonian Fluid Mechanics, 2009. **160**(1): p. 11-21.

28. Kavassalis, T.A. and P.R. Sundararajan, *A molecular-dynamics study of polyethylene crystallization.* Macromolecules, 1993. **26**(16): p. 4144-4150.

29. Liu, C. and M. Muthukumar, *Langevin dynamics simulations of early-stage polymer nucleation and crystallization.* The Journal of Chemical Physics, 1998. **109**(6): p. 2536-2542.

30. Hu, W., *Chain folding in polymer melt crystallization studied by dynamic Monte Carlo simulations.* The Journal of Chemical Physics, 2001. **115**(9): p. 4395-4401.

31. Meyer, H. and F. Muller-Plathe, *Formation of Chain-Folded Structures in Supercooled Polymer Melts Examined by MD Simulations.* Macromolecules, 2002. **35**(4): p. 1241-1252.

32. Yamamoto, T., *Molecular dynamics simulations of steady-state crystal growth and homogeneous nucleation in polyethylene-like polymer.* The Journal of Chemical Physics, 2008. **129**(18): p. 184903-11.

33. Yamamoto, T., *Molecular dynamics simulations of polymer crystallization in highly supercooled melt: Primary nucleation and cold crystallization.* The Journal of Chemical Physics, 2010. **133**(3): p. 034904-10.

34. Meyer, H. and J. Baschnagel, *Structure formation of supercooled polymers in confined geometries -- A molecular-dynamics simulation study.* The European Physical Journal E, 2003. **12**(1): p. 147-151.

35. Miura, T. and M. Mikami, *Molecular dynamics study of crystallization of polymer systems confined in small nanodomains.* Physical Review E, 2007. **75**(3): p. 031804.

36. Everaers, R., et al., *Rheology and Microscopic Topology of Entangled Polymeric Liquids.* Science, 2004. **303**(5659): p. 823-826.

37. Stephanou, P.S., et al., *Quantifying chain reptation in entangled polymer melts: Topological and dynamical mapping of atomistic simulation results onto the tube model.* The Journal of Chemical Physics, 2010. **132**(12): p. 124904-16.

38. Hoffman, J.D. and J.J. Weeks, *Rate of Spherulitic Crystallization with Chain Folds in Polychlorotrifluoroethylene.* The Journal of Chemical Physics, 1962. **37**(8): p. 1723-1741.

39. Kashchiev, D., *Nucleation: Basic Theory with Applications*. 2000, Oxford; Boston: Butterworth-Heinemann.

40. Wedekind, J., R. Strey, and D. Reguera, *New method to analyze simulations of activated processes.* The Journal of Chemical Physics, 2007. **126**(13): p. 134103-7.

41. Vehkamäki, H. and I.J. Ford, *Nucleation theorems applied to the Ising model.* Physical Review E, 1999. **59**(6): p. 6483.

42. ter Horst, J.H. and D. Kashchiev, *Determination of the nucleus size from the growth probability of clusters.* The Journal of Chemical Physics, 2003. **119**(4): p. 2241-2246.

43. Bai, X.-M. and M. Li, *Calculation of solid-liquid interfacial free energy: A classical nucleation theory based approach.* The Journal of Chemical Physics, 2006. **124**(12): p. 124707-12.

44. Paul, W., D.Y. Yoon, and G.D. Smith, *An optimized united atom model for simulations of polymethylene melts.* The Journal of Chemical Physics, 1995. **103**(4): p. 1702-1709.

45. Waheed, N., M.S. Lavine, and G.C. Rutledge, *Molecular simulation of crystal growth in n-eicosane.* The Journal of Chemical Physics, 2002. **116**(5): p. 2301-2309.

46. Waheed, N., M.J. Ko, and G.C. Rutledge, *Molecular simulation of crystal growth in long alkanes.* Polymer, 2005. **46**(20): p. 8689-8702.

47. Plimpton, S., *Fast Parallel Algorithms for Short-Range Molecular Dynamics.* Journal of Computational Physics, 1995. **117**(1): p. 1-19.

48. Gaur, U. and B. Wunderlich, *The Glass Transition Temperature of Polyethylene.* Macromolecules, 1980. **13**(2): p. 445-446.

49. Capaldi, F.M., M.C. Boyce, and G.C. Rutledge, *Molecular response of a glassy polymer to active deformation.* Polymer, 2004. **45**(4): p. 1391-1399.

50. Takeuchi, H. and R.-J. Roe, *Molecular dynamics simulation of local chain motion in bulk amorphous polymers. II. Dynamics at glass transition* Journal of Chemical Physics, 1991. **94**(11): p. 7458-7465.

51. Han, J., R.H. Gee, and R.H. Boyd, *Glass Transition Temperatures of Polymers from Molecular Dynamics Simulations.* Macromolecules, 1994. **27**(26): p. 7781-7784.

52. Harmandaris, V.A., V.G. Mavrantzas, and D.N. Theodorou, *Atomistic Molecular Dynamics Simulation of Polydisperse Linear Polyethylene Melts.* Macromolecules, 1998. **31**(22): p. 7934-7943.

53. Harmandaris, V.A., et al., *Crossover from the Rouse to the Entangled Polymer Melt Regime: Signals from Long, Detailed Atomistic Molecular Dynamics Simulations, Supported by Rheological Experiments.* Macromolecules, 2003. **36**(4): p. 1376-1387.

54. Pearson, D.S., et al., *Viscosity and self-diffusion coefficient of linear polyethylene.* Macromolecules, 1987. **20**(5): p. 1133-1141.

55. Raju, V.R., et al., *Properties of amorphous and crystallizable hydrocarbon polymers. I. Melt rheology of fractions of linear polyethylene.* Journal of Polymer Science: Polymer Physics Edition, 1979. **17**(7): p. 1183-1195.

56. Kataoka, T. and S. Ueda, *Viscosity–molecular weight relationship for polydimethylsiloxane.* Journal of Polymer Science Part B: Polymer Letters, 1966. **4**(5): p. 317-322.

57. Wunderlich, B. and C.M. Cormier, *Heat of fusion of polyethylene.* Journal of Polymer Science Part A-2: Polymer Physics, 1967. **5**(5): p. 987-988.

58. Massa, M.V., J.L. Carvalho, and K. Dalnoki-Veress, *Confinement Effects in Polymer Crystal Nucleation from the Bulk to Few-Chain Systems.* Physical Review Letters, 2006. **97**(24): p. 247802.

59. Nishi, M., et al., *Molecular Weight Dependence of Primary Nucleation Rate of Polyethylene I. An Extended Chain Single Crystal.* Polymer Journal, 1999. **31**(9): p. 749-758.

60. Ghosh, S.K., et al., *Power Law of Molecular Weight of the Nucleation Rate of Folded Chain Crystals of Polyethylene.* Macromolecules, 2002. **35**(18): p. 6985-6991.

61. Kraack, H., M. Deutsch, and E.B. Sirota, *n-Alkane Homogeneous Nucleation: Crossover to Polymer Behavior.* Macromolecules, 2000. **33**(16): p. 6174-6184.

62. Hu, W., *Intramolecular Crystal Nucleation*, in *Progress in Understanding of Polymer Crystallization*, G. Reiter and G. Strobl, Editors. 2007, Springer Berlin / Heidelberg. p. 47-63.

63. Wunderlich, B., *Molecular nucleation and segregation.* Faraday Discussions of the Chemical Society, 1979. **68**(0): p. 239-243.

64. Yoon, D.Y. and P.J. Flory, *Small-angle neutron scattering by semicrystalline polyethylene.* Polymer, 1977. **18**(5): p. 509-513.

65. Spyriouni, T., I.G. Economou, and D.N. Theodorou, *Thermodynamics of Chain Fluids from Atomistic Simulation: A Test of the Chain Increment Method for Chemical Potential.* Macromolecules, 1997. **30**(16): p. 4744-4755.

66. de Pablo, J.J., M. Laso, and U.W. Suter, *Estimation of the chemical potential of chain molecules by simulation.* The Journal of Chemical Physics, 1992. **96**(8): p. 6157-6162.

67. Kuppa, V.K., P.J. in 't Veld, and G.C. Rutledge, *Monte Carlo Simulation of Interlamellar Isotactic Polypropylene.* Macromolecules, 2007. **40**(14): p. 5187-5195.

68. Barham, P.J., et al., *The supercooling dependence of the initial fold length of polyethylene crystallized from the melt: unification of melt and solution crystallization.* Journal of Materials Science, 1985. **20**(5): p. 1625-1630.

69. Hütter, M., P.J. in 't Veld, and G.C. Rutledge, *Polyethylene {201} crystal surface: interface stresses and thermodynamics.* Polymer, 2006. **47**(15): p. 5494-5504.

70. Hoffman, J.D., *Role of reptation in the rate of crystallization of polyethylene fractions from the melt.* Polymer, 1982. **23**(5): p. 656-670.

71. Numan Waheed, G.C.R., *Crossover behavior in crystal growth rate from <I>n</I>-alkane to polyethylene.* Journal of Polymer Science Part B: Polymer Physics, 2005. **43**(18): p. 2468-2473.

72. Okada, K., et al., *Size distribution and shape of nano-nucleus of polyethylene simultaneously determined by SAXS.* Polymer, 2007. **48**(1): p. 382-392.

73. Hoffman, J.D., *The relationship of C_inf to the lateral surface free energy .sigma.: estimation of C_inf for the melt from rate of crystallization data.* Polymer, 1992. **33**(12): p. 2643-2644.

74. Hoffman, J.D., et al., *Relationship between the lateral surface free energy .sigma. and the chain structure of melt-crystallized polymers.* Macromolecules, 1992. **25**(8): p. 2221-2229.

75. Zhuravlev, E., et al., *Kinetics of nucleation and crystallization in poly(ε-caprolactone) (PCL).* Polymer, 2011. **52**(9): p. 1983-1997.

76. Loo, Y.-L., R.A. Register, and A.J. Ryan, *Polymer Crystallization in 25-nm Spheres.* Physical Review Letters, 2000. **84**(18): p. 4120-4123.

For Table of Contents Only